Cation Distribution in $LiMgVO_4$ and $LiZnVO_4$: Structural and Spectroscopic Study

D. Capsoni,[†] M. Bini,[†] V. Massarotti,*[,†] P. Mustarelli,[†] F. Belotti,[†] and P. Galinetto[‡]

Dipartimento di Chimica Fisica, "M. Rolla" dell'Università, viale Taramelli 16, 27100 Pavia, and CNISM - Dipartimento di Fisica, "A. Volta" dell'Università, via Bassi 6, 27100 Pavia

Received: December 6, 2005; In Final Form: January 30, 2006

The room temperature cation occupancy in $LiMgVO_4$ and $LiZnVO_4$ crystallographic sites is obtained by means of the combined use of X-ray powder diffraction (XRPD), ^{7}Li and ^{51}V magic angle spinning nuclear magnetic resonance (MAS NMR), and micro-Raman measurements. In the $LiMgVO_4$ *Cmcm* orthorhombic structure, the 4*c* (C_{2v} symmetry) tetrahedral vanadium site is fully ordered; on the contrary, the Li 4*c* tetrahedral site and the 4*b* (C_{2h} symmetry) Mg octahedral site display about 22% of reciprocal cationic exchange. Higher cationic disorder is observed in $LiZnVO_4$: the three cations can distribute on the three tetrahedral and distinct sites of the R-3 structure. XRPD and MAS NMR analysis results highly agree for what concerns vanadium ion distribution on the three cationic sites (about 25, 26, and 47%). From the full profile fitting of XRPD patterns with the Rietveld method, it is also obtained that Li^+ displays a slightly preferred occupation of the T1 position (∼55%) and Zn^{2+} of the T2 position (∼46%). The vibrational spectra of the two compounds are characterized by different peak positions and broadening of the Raman modes, reflecting the cation distribution and the local vibrational unit distortion. A comparison is also made with recent Raman results on Li_3VO_4. High temperature XRPD measurements rule out possible structural transitions up to 673 K for both compounds.

Introduction

$LiMgVO_4$ and $LiZnVO_4$ are vanadate compounds widely used in electrochemical devices[1,2] and as humidity sensors;[3−5] moreover, interesting properties are related to the luminescence due to the tetrahedrally coordinated V^{5+} ions.[6−8] Despite the large interest for both applicative and basic research aspects, some structural information and in particular the cation distribution in these substituted lithium vanadate systems remain still under debate.

The $LiMgVO_4$ compound was formerly assigned to the olivine group,[9,10] but further spectroscopic and powder X-ray diffraction measurements[11,12] invalidated the previous assignment to the olivine *Pnma* space group on the basis of the evidence of some extra lines. The complete structural determination was obtained by neutron diffraction study.[13] The *Cmcm* orthorhombic space group was attributed to this compound: Mg ions occupy 4*b* (C_{2h} symmetry) octahedral sites, while Li and V occupy two different 4*c* (C_{2v} symmetry) tetrahedral sites. Possible disorder between Mg and Li was excluded on the grounds of the occupancy factors of neutron Rietveld refinement.

$LiZnVO_4$ displays a trigonal $BeSi_2O_4$ phenakite-type structure,[9,14,15] where the cations occupy three tetrahedral sites. However, two space groups, R3 and R-3, are compatible with the observed systematic extinctions, with the R3 form being preferred in the ordered phenakite form, like in the $LiZnPO_4$ compound.[16] A recent study of the $LiZnV_{1-x}P_xO_4$ ($x \leq 0.6$) system proposed an R3 space group for $LiZnVO_4$ and a possible ferroelectric−paraelectric phase transition at about 488 K, as suggested by the temperature behavior of the dielectric constant.[14] On the other hand, the Raman modes may be assigned by referring to an R-3 space group.[9] To our knowledge, a definitive ion position assignment is not reported. In effect, the phenakite-type materials can easily display cationic disorder, and this fact influences the possibility to successfully explain the compound structures.

The aim of the present work is to investigate the $LiMgVO_4$ and $LiZnVO_4$ structures, in particular gaining new insights into the cation distribution by the combined use of X-ray powder diffraction (XRPD), micro-Raman measurements, and ^{7}Li and ^{51}V magic angle spinning nuclear magnetic resonance (MAS NMR). Moreover, a discussion both on the distortion in tetrahedral V and Li sites and on the degree of cation mixing is carried out in comparison with the recently studied pure and Cr doped Li_3VO_4.[17] In this orthorhombic structure, the dopant substitution can take place on both Li and V sites: this fact plays an important role in the structure and physical properties of this material.

High temperature (HT) XRPD measurements are also carried out to investigate the presence of possible phase transitions in both compounds.

Experimental Section

Both $LiMgVO_4$ and $LiZnVO_4$ were prepared by solid state synthesis from a starting mixture of Li_2CO_3 (Aldrich, 99.6%), V_2O_5 (Aldrich, 99.6%), and MgO (Merck for analysis) or ZnO (Carlo Erba for analysis) in the proper amounts. The mixed powders were ground, pelletized, and treated in Au foil for 24 h at 1073 K, cooled in 24 h to 853 K, maintained for 24 h at 853 K, and finally slowly cooled to room temperature (RT).

XRPD measurements were performed in air at RT and at different temperatures up to 673 K on a Bruker D5005 diffractometer (Bragg−Brentano geometry) with Cu Kα radiation, a Ni filter, and a position sensitive detector (PSD). For HT measurements, an Anton Paar HTK 1200 polythermal

* Corresponding author. Phone: 39-382-987203. Fax: 39-382-987575. E-mail: vincenzo.massarotti@unipv.it.
[†] "M. Rolla" dell'Università.
[‡] "A. Volta" dell'Università.

10.1021/jp057088t CCC: $33.50
Published on Web 02/24/2006

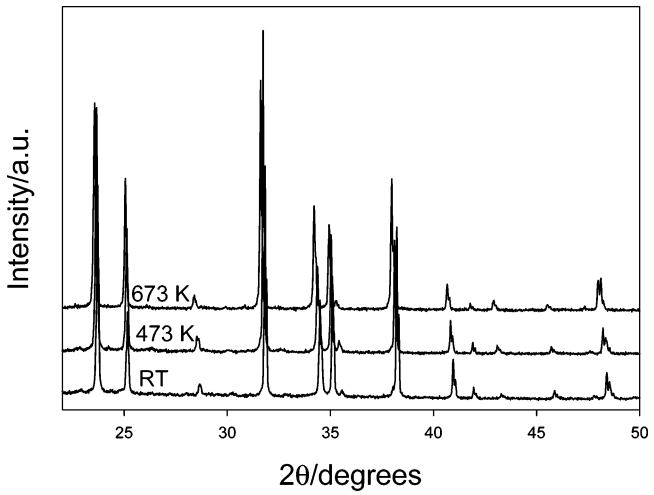

Figure 1. XRPD patterns of $LiMgVO_4$ at RT, 473 K, and 673 K.

attachment was used. Rietveld structural and profile refinement was carried out by means of the FULLPROF program[18] on RT patterns.

Micro-Raman measurements were carried out at RT by using a Labram Dilor H10 spectrometer equipped with an Olympus HS BX40 microscope. A HeNe laser beam (632.8 nm) was employed as exciting light with a power less than 10 mW at the sample. The microscope, coupled confocally to the spectrograph with a 100× objective of numerical aperture 0.9, collected the backscattered Raman light from the sample irradiated with a laser spot with a diameter of ~1 μm.

NMR measurements were performed at RT on a AMX400WB spectrometer (Bruker) based on a 9.4 T magnet. MAS spectra were acquired with a 4 mm probehead (Bruker), equipped with cylindrical zirconia rotors and a boron nitride stator. ^{51}V MAS NMR spectra were collected at 105.19 MHz. The samples were spun at 7−12 kHz, and the data were averaged over 12K acquisitions using a single-pulse sequence, with a 15° pulse of 0.5 μs and a recycle time of 1 s. The baseline distortions were corrected by linear prediction of the first 10−15 points of the FIDs, followed by baseline correction (WINNMR software, Bruker). The simulations of the spectra were performed by using the WSOLIDS package.[19] ^7Li MAS NMR measurements were performed at 155.6 MHz. The samples were spun at 10 kHz, and the data were averaged over 32 acquisitions using a single-pulse sequence, with a 90° pulse of 3 μs and a recycle time of 10 s. The spectra were referenced to an external sample of 1.0 M LiCl in H_2O. The spectra were processed without left shifts, by applying a spline baseline correction.

Results

$LiMgVO_4$. The RT XRPD pattern of the sample, reported in Figure 1, shows the only peaks pertinent to the orthorhombic form reported in the literature[13] (JCPDS 49-0263). The Rietveld refinement was performed on the basis of the literature structural model with Li and V on two different tetrahedral sites and Mg octahedrally coordinated.[13] On the basis of the simulation by using an ordered cationic distribution on the pertinent sites, it can be observed that the experimental intensity of *h*00, 0*k*0, and 110 reflections is systematically higher than the calculated one. It has been demonstrated that the intensity of the 110 reflection, at $2\theta = 18.80°$, is markedly influenced by the mixing degree between Li and Mg in the pertinent sites, while no mixing degree can reduce the observed intensity discrepancies of *h*00 and 0*k*0 reflections. For these reflection planes, we hypothesize

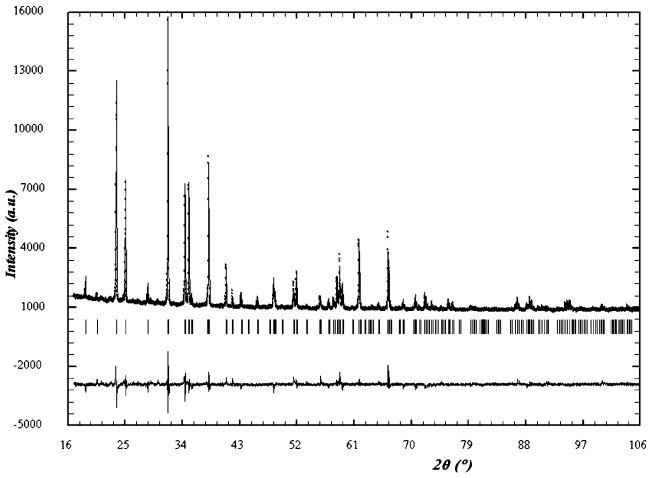

Figure 2. Observed (points) and calculated (line) XRPD patterns of the $LiMgVO_4$ sample. The peak positions (vertical bars) and the difference curve are also shown (bottom).

TABLE 1: Lattice Parameters, Ion Fractional Coordinates, Thermal Factors, Cation Occupancies, and Discrepancy Factors Obtained from Rietveld Refinement on $LiMgVO_4$

a, *b*, *c*/Å	5.6314(3), 8.6226(4), 6.2439(3)
Mg site	
x, *y*, *z*	0.0, 0.5, 0.0
B/Å^2	1.282(1)
Mg and Li occupancy	0.779(3), 0.221(3)
Li site	
x, *y*, *z*	0.0, 0.1982(3), 0.25
B/Å^2	1.793(3)
Li and Mg occupancy	0.779(3), 0.221(3)
V site	
x, *y*, *z*	0.0, 0.8517(1), 0.25
B/Å^2	0.755(1)
O1 site	
x, *y*, *z*	0.2573(2), 0.4741(1), 0.25
B/Å^2	1.511(1)
O2 site	
x, *y*, *z*	0.0, 0.2426(1), 0.5310(2)
B/Å^2	−0.138(1)
R_{wp}	5.25
R_B	12.3
χ	1.75

the presence of preferred orientation effects. The Rietveld refinement of global, profile, and structural parameters is performed by taking into account the *h*00 March−Dollase preferred orientation model;[18] the results of structural parameters, conventional Rietveld discrepancy factors[18] R_{wp} and R_B, and the goodness of fit, χ, are reported in Table 1. The comparison between observed and calculated patterns is shown in Figure 2, together with the difference curve and the positions of the Bragg peaks. The lattice parameters and atomic coordinates (Table 1) are in good agreement with the literature ones,[13] but for the *y* value of the Li ion; the thermal factors are reliable, and only the O2 ion shows a small negative value. For what concerns the site occupancies, the most satisfactory results were obtained by allowing some cationic mixing in both octahedral Mg and tetrahedral Li sites. Evidence of about 20% of cationic mixing between Mg and Li is obtained (see Table 1), while the vanadium ions completely occupy their tetrahedral site. Other cation distribution models and/or different preferred orientation directions lead to higher values of both discrepancy factors and goodness of fit. In addition, the thermal factors of Li and O1 ions reach negative and highly positive values, respectively. The ion−ion distances determined on the grounds of the refined ion positions for first, second, and third cation coordination are reported in Table 2. Very similar values of Mg−O bond lengths

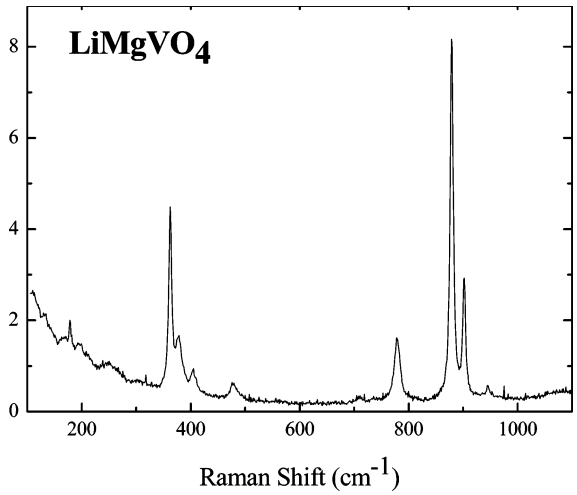

Figure 3. Raman spectrum of $LiMgVO_4$ measured at RT.

TABLE 2: Number and Distances of First, Second, and Third Coordination Shell for Cationic Sites in $LiMgVO_4$

central atom	coordinated atom	ion−ion distances (Å)
Mg	4 × O1	2.141
	2 × O2	2.228
	2 × Mg	3.122
	6 × Li	2 × 3.035, 4 × 3.645
	6 × V	2 × 3.411, 4 × 3.464
Li	2 × O1	2.367
	2 × O2	1.796
	6 × Mg	2 × 3.035, 4 × 3.645
	6 × Li	4 × 4.298, 2 × 4.630
	5 × V	2.988, 2 × 3.111, 2 × 3.151
V	2 × O1	1.727
	2 × O2	1.591
	6 × Mg	2 × 3.411, 4 × 3.464
	5 × Li	2.988, 2 × 3.111, 2 × 3.151
	6 × V	2 × 4.036, 4 × 4.555

TABLE 3: Temperature Dependence of Lattice Parameters and Cell Volumes in $LiMgVO_4$ and $LiZnVO_4$

T/K	*a*/Å	*b*/Å	*c*/Å	*V*/Å^3
		$LiMgVO_4$		
473	5.6453(3)	8.6347(5)	6.2644(4)	305.36(6)
673	5.6651(3)	8.6546(6)	6.2917(4)	308.48(6)
		$LiZnVO_4$		
373	14.1876(2)		9.4911(2)	1654.49(8)
473	14.1985(2)		9.5031(2)	1659.13(8)
573	14.2106(2)		9.5152(2)	1664.08(8)
673	14.2220(2)		9.5257(2)	1668.59(8)

are observed, confirming the presence of rather regular octahedra in the crystal structure; distorted and non-homogeneous values of bond lengths are instead obtained on tetrahedral sites, in particular on Li ones.

In Figure 1, the HT XRPD patterns are reported and compared. Table 3 reports lattice parameters and volume values at different temperatures: it is demonstrated that the structure is stable in the whole examined temperature range.

In Figure 3, a representative Raman spectrum for the $LiMgVO_4$ sample is reported in the energy region 100−1200 cm^{-1}. The main features are observable in two different vibrational energy ranges. In the high energy part of the spectrum, the most intense Raman lines are measured respectively at ∼778, ∼878, and ∼902 cm^{-1}. An additional weaker Raman peak is observed at 945 cm^{-1}. In the frequency region between 350 and 500 cm^{-1}, other significant Raman modes are measured. Among these, the most intense is observed at 363 cm^{-1} and the other at 378, 405, and 479 cm^{-1}, respectively.

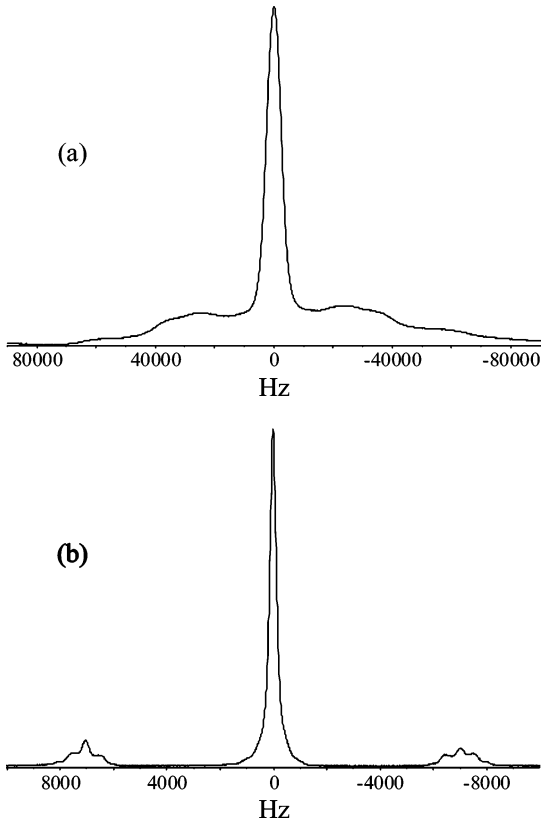

Figure 4. (a) Wide-line and (b) MAS ^{7}Li NMR spectra of $LiMgVO_4$.

The spectra have also been collected from different points of the powder to test the sample homogeneity. No difference among spectra was detected during micro-Raman mapping, indicating a high degree of homogeneity and the absence of impurity phases.

Figure 4 shows the wide-line (a) and MAS (b) ^{7}Li NMR spectra. The wide-line spectrum is characterized by a central line with a full width at half-height (fwhh) of about 6 kHz and by satellite transitions that give a value of the quadrupolar coupling constant, C_{qq}, of ∼130 kHz, which is typical of lithium compounds.[20] The MAS spectrum (part b) shows a relatively narrow line (fwhh ≅ 290 Hz) that is well fitted by a single peak with $C_{qq} = 130$ kHz, quadrupolar asymmetry $\eta = 0.0$, and Lorentzian broadening $\Delta_L = 285$ Hz. These results suggest that all lithium cations are nearly equivalent from a magnetic point of view. However, because of the low nuclear quadrupole moment of ^{7}Li and the low ^{7}Li chemical shift range in diamagnetic compounds (≤5 ppm), we cannot rule out cation mixing between Li and Mg sites.

Figure 5 displays the entire ^{51}V MAS spectrum together with an enlarged portion showing the spectral region of the isotropic peak. The overall spectrum is characterized by a low chemical shift anisotropy, as expected for orthovanadates.[21,22] A rough simulation of the isotropic peak with a single quadrupolar site gives the following values: $C_{qq} = 3 \pm 0.5$ MHz and $\eta = 0.5 \pm 0.3$, which are reasonable for an orthovanadate compound. While the extraction of the quadrupolar parameters does require the best fit of the overall spectrum,[23] which is not allowed by our software, the shape of the peak attributed to the central transition strongly suggests that all of the vanadium cations are in the same crystallographic site, in agreement with the result of the Rietveld refinement.

$LiZnVO_4$. The RT $LiZnVO_4$ XRPD pattern reported in Figure 6 shows the only peaks pertinent to the trigonal phenakite-type structure[9,16] (JCPDS 38-1332). The reliability of both the space

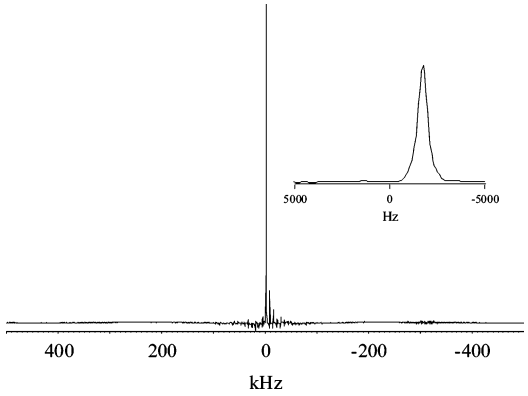

Figure 5. ^{51}V MAS entire spectrum of $LiMgVO_4$. The inset shows an enlarged portion of the isotropic peak spectral region.

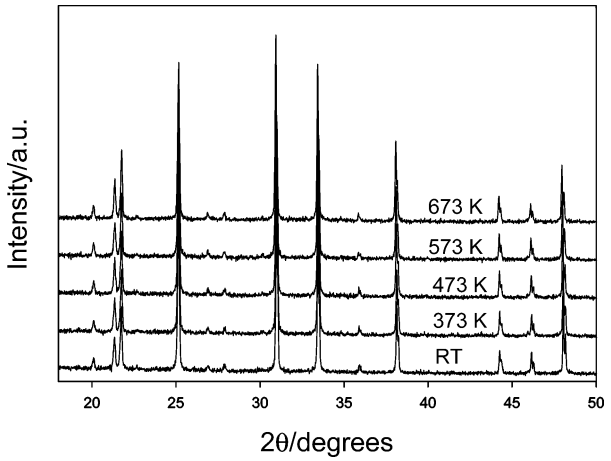

Figure 6. XRPD patterns of $LiZnVO_4$ at RT and HT up to 673 K.

groups R3 (ordered phenakite structure, $LiZnPO_4$ type[16]) and R-3 (phenakite $SiBe_2O_4$ type[9]) and the cation distribution on the tetrahedral sites was preliminary tested by means of the Rietveld refinement. A comparison between the different models was performed on the basis of the conventional Rietveld discrepancy factors and especially of the χ value at the same refinement level where only global and lattice parameters were varied. The highest χ value is obtained when considering $LiZnVO_4$ isostructural with $LiZnPO_4$[16] ($\chi = 6.0$), while $\chi = 4.6$ is obtained in the case of a random distribution of cations in the same R3 symmetry. In any case, the best values are reached by using the R-3 space group. Each cation was positioned in turn on the three different tetrahedral sites T1, T2, and T3, obtaining χ values in the range 4.7−5.2. A significant lowering of the goodness of fit ($\chi = 3.13$) was finally obtained by randomizing the cations on the three tetrahedral sites and permitting the insertion of a great degree of disorder in the structure. The fit was completed by refining profile parameters, atomic positions, thermal factors and cation occupancies. The results are reported in Table 4: a goodness of fit of 1.82 is reached. The comparison between observed and calculated patterns is shown in Figure 7 together with the difference curve and the Bragg peak positions. The lattice parameters, atomic coordinates, and occupancies are reliable with respect to their standard deviations (Table 4); the cation thermal factors are positive, while the pertinent values for O1 and O2 are negative. This fact can reflect the correlation with occupancy factors and positions in partially disordered samples. Table 5 reports the ion−ion distances for the first, second, and third coordination of cations deduced by the cation coordinate

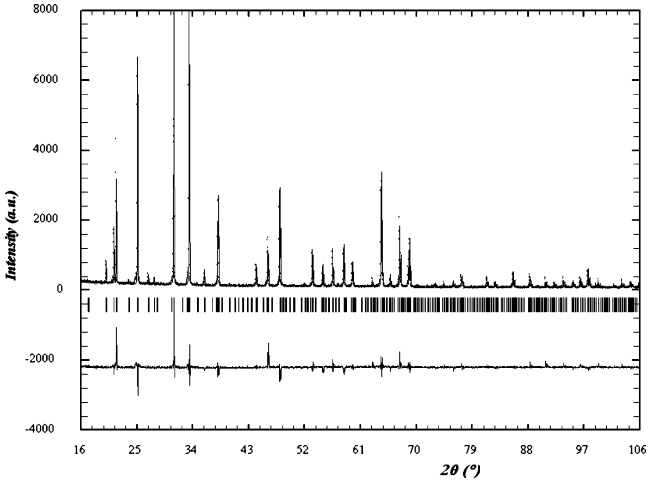

Figure 7. Observed (points) and calculated (line) XRPD patterns of the $LiZnVO_4$ sample. The peak positions (vertical bars) and the difference curve are also shown (bottom).

TABLE 4: Lattice Parameters, Ion Fractional Coordinates, Thermal Factors, Cation Occupancies, and Discrepancy Factors Obtained from Rietveld Refinement on $LiZnVO_4$

a, *c*/Å	14.1857(1), 9.4879(1)
T1	
x, *y*, *z*	0.1918(2), 0.9769(2), 0.7471(5)
B	0.12(6)
N (V)	0.251(2)
N (Zn)	0.198(2)
N (Li)	0.553(2)
T2	
x, *y*, *z*	0.1957(2), 0.9825(2), 0.4141(3)
B	0.05(5)
N (V)	0.255(5)
N (Zn)	0.465(4)
N (Li)	0.291(4)
T3	
x, *y*, *z*	0.1880(2),0.9772(1), 0.0808(3)
B	0.84(6)
N (V)	0.468(5)
N (Zn)	0.319(4)
N (Li)	0.204(4)
O1	
x, *y*, *z*	0.2145(3), 0.1322(3), 0.7518(9)
B	−0.89(8)
O2	
x, *y*, *z*	0.3371(4), −0.0103(4), 0.7486(11)
B	−1.74(6)
O3	
x, *y*, *z*	0.1154(5), 0.8976(4), 0.9293(9)
B	0.74(14)
O4	
x, *y*, *z*	0.1235(4), 0.9056(5), 0.5602(7)
B	−0.15(14)
R_{wp}	14.0
R_B	13.5
χ	1.82

refinement. Among the rather regular tetrahedra obtained, the $T1O_4$ one results in being the most expanded.

The high temperature XRPD measurements up to 673 K were performed to analyze the possible structural transition, previously suggested on the grounds of the dielectric constant trend with temperature, in the $LiZnVO_4$−$LiZnPO_4$ system.[14] The patterns are shown in Figure 6. Neither new peaks nor intensity variations are observed with temperature, confirming that no structural change takes place in this temperature range. The lattice parameters and cell volume values at different temperatures are reported in Table 3.

A representative Raman spectrum for the $LiZnVO_4$ compound is reported in Figure 8. Also, for this sample, the Raman features

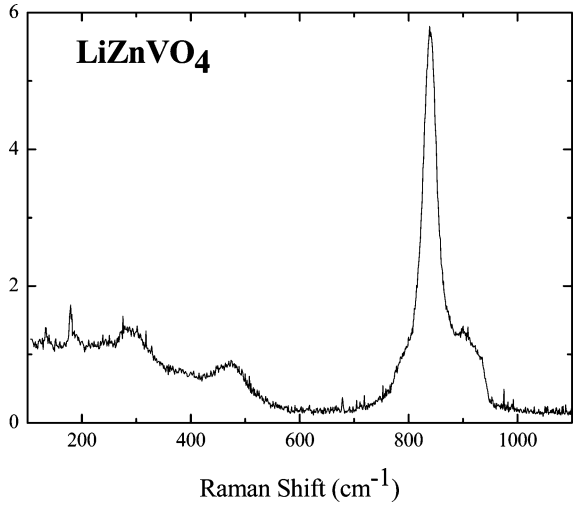

Figure 8. Raman spectrum of $LiZnVO_4$ measured at RT.

TABLE 5: Number and Distances of First, Second, and Third Coordination Shell for Cationic Sites in $LiZnVO_4$

central atom	coordinated atom	ion−ion distances (Å)
T1	O1	2.053
	O2	1.958
	O3	2.026
	O4	2.055
	3 × T1	4.115, 2 × 4.502
	5 × T2	3.164, 3.230, 3.238, 3.331, 4.477
	6 × T3	3.159, 3.277, 3.290, 3.329, 4.081, 4.553
T2	O1	1.821
	O2	1.904
	2 × O4	1.727, 1.885
	5 × T1	3.164, 3.230, 3.238, 3.331, 4.477
	5 × T2	2 × 3.333, 4.182, 2 × 4.496
	4 × T3	3.169, 3.234, 4.180, 4.570
T3	O1	1.785
	O2	1.770
	2 × O3	1.796, 1.820
	6 × T1	3.159, 3.277, 3.290, 3.329, 4.081, 4.553
	4 × T2	3.170, 3.234, 4.180, 4.570
	6 × T3	2 × 3.217, 2 × 4.601, 2 × 4.913

allow the vibrational response to be split into two parts: in the lower energy part of the spectrum, weak and broadened features are observed, peaked approximately at 290 and 475 cm^{-1}. At higher energy, only one intense mode is visible, peaked at 838 cm^{-1}. This Raman line is almost symmetric but is clearly accompanied, at lower signal level, by appreciable shoulders, in particular at higher energies. Also, in this case, Raman mapping evidenced a good homogeneity and absence of host phases.

Figure 9 shows the wide-line (a) and MAS (b) ^{7}Li NMR spectra. The wide-line spectrum is characterized by a central line with fwhh $\cong$ 5.8 kHz, which is very similar to that observed for $LiMgVO_4$. The satellite transitions, in contrast, have quite a different shape that points to $C_{qq} \sim 60$ kHz, which is nearly half of that observed for $LiMgVO_4$. The MAS spectrum (b) shows a single isotropic peak with fwhh = 485 Hz, ~70% larger than that of $LiMgVO_4$, that can be well fitted by a Gaussian/Lorentzian curve with a G/L ratio of ~60%. These findings point to a distribution of the lithium cations that is more disordered than that of $LiMgVO_4$, in agreement with the XRPD Rietveld refinement.

Additional information can be obtained by ^{51}V NMR. Figure 10 shows the entire ^{51}V MAS spectrum, and the insets report the isotropic peak (a) and its power spectrum (b). While the

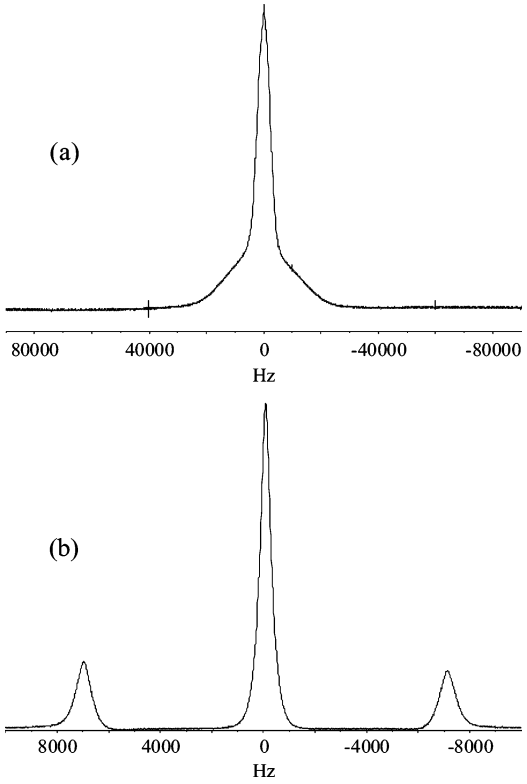

Figure 9. (a) Wide-line and (b) MAS ^{7}Li NMR spectra of $LiZnVO_4$.

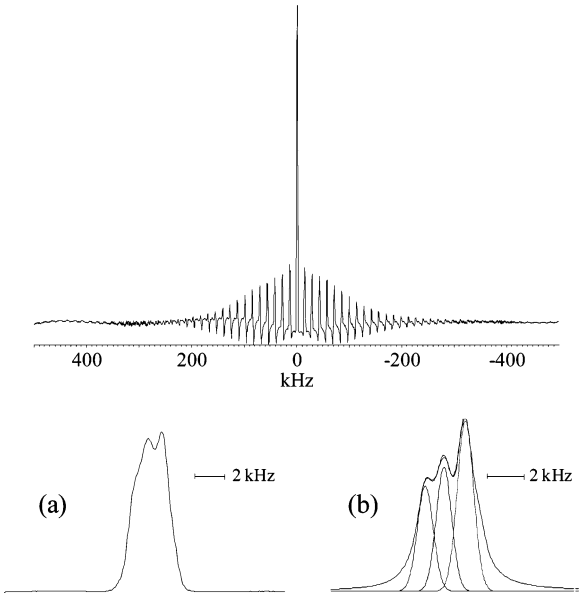

Figure 10. ^{51}V MAS entire spectrum of $LiZnVO_4$. Inset a reports the isotropic peak and inset b its power spectrum, together with its deconvolution with three Gaussian functions.

attempt to fit the isotropic peak in terms of a single quadrupolar site did not give good results, a fit with Gaussian functions performed on the power spectrum did put into evidence three components with normalized areas of 24, 26, and 44%, respectively (see caption), that can be attributed to V atoms distributed over the T1, T2, and T3 sites, in good agreement with the Rietveld refinement of the XRPD data. Since our Gaussian fits do not consider the possible second-order quadrupolar broadening of the MAS lines, we will consider them to be only qualitative. A correct extraction of the quadrupolar parameters of the different V sites can be obtained by means

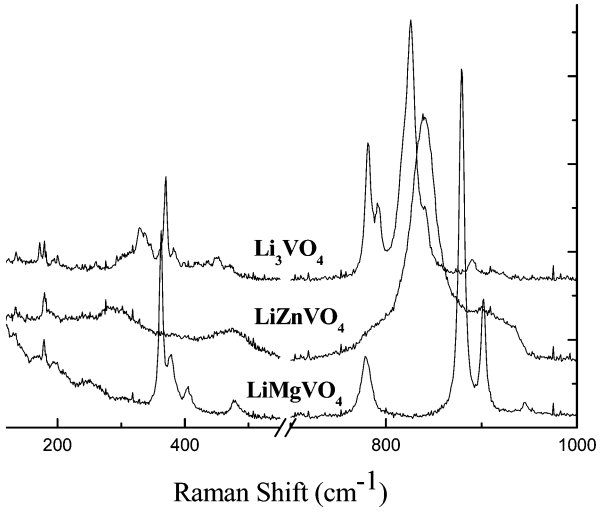

Figure 11. Comparison between the Raman spectra of $LiMgVO_4$ and $LiZnVO_4$ with the spectrum of the Li_3VO_4 compound.[17] All of the spectra have been collected under the same experimental conditions.

of MQMAS experiments,[21] which are not possible with the current setup of our NMR spectrometer.

Discussion and Conclusions

The above-reported results allow us to discuss the $LiMgVO_4$ and $LiZnVO_4$ structures, gaining new insights into the pertinent cation distribution. It is quite difficult to explain satisfactorily the Raman results for the considered samples on the basis of a lattice-dynamical interpretation of the modes extended to the whole crystal and of space group and site symmetry considerations. From vibrational Raman spectra, we notice that the present Raman results are in good agreement with previously reported data[9,11] for the $LiMgVO_4$ sample.

In the case of $LiZnVO_4$, starting from the phenakite structure and the space group R3, more than 40 Raman modes should be measured.[25] In contrast, few Raman peaks have been observed. Some Raman modes can be intrinsically weak due to a small oscillator strength, but generally, it can be said that the disorder tends to weaken the selection rules, affecting markedly the Raman spectra. The results on both studied compounds can be explained by using a local environment model including TO_4 tetrahedra and MO_6 octahedra as vibrational units. On this basis and taking into account previous studies on vanadate compounds[17,26] having different structures, it is possible to assign the high energy modes to vibrations involving stretching motion of the TO_4 groups. For the sake of comparison, we can consider the Raman spectra obtained in other compounds having different crystalline structures but in which it is possible to isolate the contribution to the vibrational spectrum of the TO_4 tetrahedral units, as in Li_3VO_4 and $LiNiVO_4$ compounds.[17,26] Figure 11 shows the comparison between Raman spectra of the present samples and Li_3VO_4. For what concerns signals arising from the TO_4 tetrahedral units, it can be observed that $LiMgVO_4$ exhibits Raman lines with a smaller bandwidth and larger splitting if compared with Li_3VO_4. The splitting between the most intense mode and the lowest energy mode (at 779 cm^{-1} for both samples) in this spectral region is 100 cm^{-1} for the Mg sample and 50 cm^{-1} for Li_3VO_4. In addition, if we consider the line widths of the most intense mode for the three reported samples, we obtain 7.5, 15, and 30 cm^{-1} for the $LiMgVO_4$, Li_3VO_4, and $LiZnVO_4$ samples, respectively. These results can be explained by taking into account the Li−O and V−O bond lengths (see Table 2 and ref 17). The LiO_4 and VO_4 tetrahedral units for the $LiMgVO_4$ sample are particularly distorted due to rather different bond lengths being within the same vibrational unit (Table 2); the same tetrahedra are instead regular with homogeneous bond lengths for Li_3VO_4.[17] The lower degree of symmetry of the vibrational unit in $LiMgVO_4$ causes an increase of the splitting and a narrowing of the modes. As a consequence, the different full widths at half-maximum of the vibrational modes in the two samples are due more to the main effect of environment distortion than to the different degree of cation mixing observed only on Li sites in $LiMgVO_4$. Therefore, comparing $LiMgVO_4$ and Li_3VO_4, one can say that a low degree of disorder in the cation distribution has an activating effect in Raman signal due to a greater anisotropy in bond lengths, but when the disorder in cationic distribution becomes more pronounced, as for the $LiZnVO_4$ sample, there is a relaxation of Raman selection rules with a consequent decrease and broadening of spectral features. This effect is more pronounced in the spectral region below 500 cm^{-1}, where the Raman signals are probably due to lattice modes instead of internal modes. The vibrations due to internal modes can be considered as less sensitive to the cationic disorder, and the effect is appreciable analyzing the line widths and peak positions, as mentioned above. For lattice modes, the role of cationic disorder is more effective and it reflects on Raman spectra, causing practically the disappearance of the signal as for the Raman spectrum of $LiZnVO_4$. A more accurate analysis and discussion about the role of cation distribution can arise from measurements on single crystals, which, to our knowledge, are not yet available.

The structural investigation of the two studied compounds highlights a quite different degree of cationic disorder and coordination: in both cases, the tetrahedral coordination of V^{5+} ions is preserved (Tables 1, 2, 4, and 5). In $LiMgVO_4$, Li and Mg sites have different coordination; however, a mixing of about 22% (Table 1) is required to obtain the best fit between experimental and calculated XRPD patterns. On these grounds, we can put into evidence that the 110 reflection intensity represents an efficient indicator of the cation mixing degree on Li and Mg sites. Unfortunately, simulations performed on ^7Li MAS NMR signals do not univocally support the hypothesis of Li/Mg mixing. In fact, simple simulation sensitivity tests performed by changing the asymmetry parameter, η, from 0 to 1 and C_{QQ} in the range 80−130 kHz revealed only negligible effects on the MAS line shape. On the contrary, we can deduce that all of the vanadium cations fully occupy their pertinent crystallographic site (Table 1), as suggested by both XRPD and NMR results; the possible Li/Mg mixing does not cause a detectable perturbation of the next-neighbor V atoms. On the other hand, this is reasonable because of the diamagnetic nature of the cations involved in the mixing. In contrast, it was recently shown that the addition of 1 mol % erbium to rare-earth vanadates causes the appearance of a new site in the ^{51}V spectrum.[24] Also, Raman signal features support this evidence: the band peaked at 838 cm^{-1}, due to VO_4 vibration, is very narrow (Figure 3), as expected in cases of the absence of cation substitution.

In the $LiZnVO_4$ compound, the three tetrahedral cationic sites, which are crystallographically distinct, display a significant degree of mixing even if with a preference of Li on T1 (∼55%), Zn on T2 (∼46%), and V on T3 (∼47%) sites, as obtained by Rietveld refinement (Table 4). For what concerns the V content on the three sites, the values obtained by XRPD (25% on T1, 26% on T2, and 47% on T3, Table 4) are in very good agreement with the ^{51}V MAS NMR signal simulation results (24, 26, and 44%, respectively). The increased disorder in the

cation distribution is clearly reflected in the Raman spectrum (Figure 8). As a matter of fact, we observe a general broadening and weakening of signals especially for the modes around 400 cm^{-1}. Also, at high energies, the effect of disorder is appreciable because the width of the intense line at 838 cm^{-1} is, in any case, larger than the corresponding mode in the Mg sample. In addition, the large splitting observed in the Mg sample is reduced and the different stretching vibrations are characterized by similar energies, as evidenced by the presence of shoulders just below and above the main Raman peak. The Raman spectrum for $LiZnVO_4$ can therefore be justified by considering the main role played by the disorder in the occupancy of tetrahedral sites with respect to that played by the bond lengths between and within the tetrahedral reported in Table 5. The largest Li^+ ions ($r_{Li^+} = 0.59$ Å) and the smallest V^{5+} ions ($r_{V^{5+}} = 0.36$ Å) occupy preferentially the most enlarged T1 and smallest T3 tetrahedra, respectively (see Table 5). A similar effect is observed also in $LiMgVO_4$: the cell is slightly expanded with respect to the neutron diffraction data,[13] and both Li tetrahedra and Mg octahedra are enlarged. In particular, LiO_4 tetrahedra appear strongly distorted. This distortion depends on the refined *y* coordinate of the Li site (Table 1), rather different from the value reported in the literature ($y = 0.164$).[13] However, tentative simulations by imposing the literature *y* value lead to a very high and negative thermal factor on this site. It can be noted also that the VO_4 tetrahedra are significantly contracted with respect to literature data.[13] All of these observations are in agreement with the presence of some degree of cationic disorder.

For what concerns the thermal behavior of the investigated vanadates, no structural transitions are observed up to 673 K from HT XRPD data. In the case of the $LiMgVO_4$ compound, the cell volume data are obtained by using the lattice parameter values reported in Tables 1 and 3. A linear regression satisfactorily describes volume versus *T* data, and a thermal expansion coefficient of $4.72 \times 10^{-5}\ K^{-1}$ is obtained. For what concerns the $LiZnVO_4$ compound, a thermal expansion coefficient of $2.85 \times 10^{-5}\ K^{-1}$ is instead obtained. No discontinuities in the lattice parameters and cell volume trends with *T* are present in the *T* range where dielectric constant maxima were observed.[14] On the other hand, our $LiZnVO_4$ sample already shows a disordered R-3 structure at RT, differently from the sample discussed by Azrour et al.[14] where an ordered R3 structure was proposed.

In conclusion, this study demonstrates that the combined use of different spectroscopic and structural investigation techniques on structurally different vanadate compounds is extremely useful to completely characterize the different degree of cationic disorder in these samples.

NMR and XRPD measurements give quantitative results on cation distribution; in the case of the $LiZnVO_4$ compound, a total agreement of the disorder degree between the two techniques is reached, while, for the $LiMgVO_4$ sample, due to the diamagnetic nature of the cations involved in the mixing, only XRPD Rietveld refinement clearly confirms the Li/Mg exchange in the cationic sublattice. The Raman investigation shows interesting variations on line broadening on the same Raman modes in the different tetrahedral cationic sites, in particular on VO_4 modes at about 840 cm^{-1}. On the basis of these findings, a useful comparison with previously discussed vanadate compounds[17] can be carried out.

References and Notes

(1) Sigala, C.; Guyomard, D.; Piffard, Y.; Tournoux, M. *C. R. Acad. Sci., Ser. IIb: Mec., Phys., Chim., Astron.* **1995**, *320*, 523.

(2) Le Gal La Salle, A.; Verbaere, A.; Piffard, Y.; Guyomard, D. *NATO Sci. Ser., 3* **2000**, *85*, 241.

(3) Fu, G.; Chen, H.; Chen, Z.; Zhang, J.; Kohler, H. *Sens. Actuators, B* **2002**, *B81*, 308.

(4) Ying, J.; Wan, C.; He, P. *Sens. Actuators, B* **2000**, *B62*, 165.

(5) Wu, M.; Sun, H.; Li, P. *Sens. Actuators, B* **1994**, *17*, 109.

(6) Ronde, H.; Blasse, G. *J. Inorg. Nucl. Chem.* **1978**, *40*, 215.

(7) Ronde, H.; Snijders, J. G. *Chem. Phys. Lett.* **1977**, *50*, 282.

(8) Ronde, H.; Blasse, G. *J. Solid State Chem.* **1976**, *17*, 339.

(9) Corsmit, A. F.; Blasse, G. *Chem. Phys. Lett.* **1973**, *20*, 347.

(10) Blasse, G. *J. Inorg. Nucl. Chem.* **1963**, *25*, 230.

(11) Paques-Ledent, M. Th. *Chem. Phys. Lett.* **1974**, *24*, 231.

(12) Paques-Ledent, M. Th. *Chem. Phys. Lett.* **1975**, *35*, 375.

(13) Barbier, J. *Eur. J. Solid State Inorg. Chem.* **1988**, *25*, 609.

(14) Azrour, M.; El Ammari, L.; Depmeier, W.; Elouadi, B. *Ann. Chim. Sci Mater.* **1998**, *23*, 251.

(15) Blasse, G. *J. Inorg. Nucl. Chem.* **1963**, *25*, 136.

(16) Bu, X.; Gier, T. E.; Stucki, G. D. *Acta Crystallogr., Sect. C* **1996**, *52*, 1601.

(17) Massarotti, V.; Capsoni, D.; Bini, M.; Mustarelli, P.; Chiodelli, G.; Azzoni, C. B.; Galinetto, P.; Mozzati, M. C. *J. Phys. Chem. B* **2005**, *109*, 14845.

(18) Rodriguez-Carvajal, J. *Physica B* **1993**, *192*, 55.

(19) The WSOLIDS package was provided by K. Eichele. See http://casgm3.anorg.chemie.uni-tuebingen.de/klaus/soft/index.html.

(20) Mustarelli, P.; Quartarone, E.; Benevelli, F. *Mater. Res. Bull.* **1997**, *32*, 679.

(21) Lapina, O. B.; Shubin, A. A.; Khabibulin, D. F.; Terskikh, V. V.; Bodart, P. R.; Amoureux, J-. P. *Catal. Today* **2003**, *78*, 91.

(22) Nielsen, U. G.; Jakobsen, H. J.; Skibsted, J. *Solid State Nucl. Magn. Reson.* **2003**, *23*, 107.

(23) Jäger, C. In *Solid State NMR II: Inorganic Matter*; Diehl, P., et al., Eds.; Springer-Verlag: Berlin, 1994; p 133.

(24) Amantea, R.; Ghigna, P.; Mustarelli, P.; Tartara, V. *J. Solid State Chem.* **2005**, *178*, 1692.

(25) Pilati, T.; Gramaccioli, C. M.; Pezzotta, F.; Fermo, P.; Bruni, S. *J. Phys. Chem. A* **1998**, *102*, 4990.

(26) Julien, C.; Massot, M.; Perez-Vicente, C. *Mater. Sci. Eng., B* **2000**, *75*, 6.